Anal. Chem. **2010,** *82,* 4151–4157

Bipolar Ionization Source for Ion Mobility Spectrometry Based on Vacuum Ultraviolet Radiation Induced Photoemission and Photoionization

Chuang Chen,[†,‡] Can Dong,[†] Yongzhai Du,[†,‡] Shasha Cheng,[†,‡] Fenglei Han,[†,‡] Lin Li,[†] Weiguo Wang,[†] Keyong Hou,[†] and Haiyang Li*[,†]

State Key Laboratory of Molecular Reaction Dynamics, Dalian Institute of Chemical Physics, Chinese Academy of Sciences, Dalian, 116023, People's Republic of China, and Graduate School of Chinese Academy of Sciences, Beijing, 100039, People's Republic of China

A novel bipolar ionization source based on a commercial vacuum-UV Kr lamp has been developed for ion mobility spectrometry (IMS), which can work in both negative and positive ion mode. Its reactant ions formed in negative ion mode were predominantly assigned to be $O_3^-(H_2O)_n$, which is different from that of the ^{63}Ni source with purified air as carrier and drift gases. The formation of $O_3^-(H_2O)_n$ was due to the production of ozone caused by ultraviolet radiation, and the ozone concentration was measured to be about 1700 ppmv by iodometric titration method. Inorganic molecules such as SO_2, CO_2, and H_2S can be easily detected in negative ion mode, and a linear dynamic range of 3 orders of magnitude and a limit of detection ($S/N = 3$) of 150 pptv were obtained for SO_2. Its performance as a negative ion source was investigated by the detection of ammonium nitrate fuel oil explosive, *N*-nitrobis(2-hydroxyethyl)amine dinitrate, cyclo-1,3,5-trimethylene-2,4,6-trinitramine, and pentaerythritol tetranitrate (PETN) at 150 °C. The limit of detection was reached at 45 pg for PETN, which was much lower than the 190 pg using ^{63}Ni ion mobility spectrometry under the same experimental condition. Also, its performance as an ordinary photoionization source was investigated in detecting benzene, toluene, and *m*-xylene.

Ion mobility spectrometry (IMS) is widely known as an atmospheric pressure analysis technique, which can distinguish gas-phase ions based on the differences in their reduced mobilities.[1] Due to its many attractive features such as high sensitivity, fast response, and a relatively low cost, it is widely applied in the detections of explosives, drugs of abuse, and chemical warfare agents and the analyses of biological and medical samples.[1−6] Also, it has been used as a detector for a range of separation techniques including gas chromatography[7] and high-performance liquid chromatography.[8]

As one of the important parts of an IMS instrument, the ionization source determines the performance and the application fields of IMS to a great extent. The widely used ionization source, especially in commercial devices, is mainly ^{63}Ni radioactive source. The reason for adopting the ^{63}Ni source is its stability, long lifetime, and simplicity.[1] However, its applications are discouraged because of a variety of safety, environmental, and regulatory concerns related to its radioactive nature. Therefore, great efforts have been performed to search for nonradioactive ionization alternatives, for instance, the electrospray method[9,10] and the secondary electrospray method.[11,12] Beside these, optical,[13,14] corona discharge,[15−18] and glow discharge,[19,20] etc., were also used for the IMS analyses. Among them, a well-known nonradioactive alternative of the ^{63}Ni source is the ultraviolet radiation photoionization source.[21,22] It can be applied to ionize compounds with ionization potentials (IP) below the photon

* To whom all correspondence should be addressed. Phone: +86 411 84379509. Fax: +86 411 84379517. E-mail: hli@dicp.ac.cn.
† Dalian Institute of Chemical Physics.
‡ Graduate School of Chinese Academy of Sciences.

(1) Eiceman, G. A.; Karpas, Z. *Ion Mobility Spectrometry*, 2nd ed.; CRC Press: Boca Raton, FL, 2005.
(2) Borsdorf, H.; Eiceman, G. A. *Appl. Spectrosc. Rev.* **2006**, *41*, 323–375.
(3) Westhoff, M.; Litterst, P.; Freitag, L.; Urfer, W.; Bader, S.; Baumbach, J. I. *Thorax* **2009**, *64*, 744–748.
(4) Myung, S.; Wiseman, J. M.; Valentine, S. J.; Takats, Z.; Cooks, R. G.; Clemmer, D. E. *J. Phys. Chem. B* **2006**, *110*, 5045–5051.
(5) Dwivedi, P.; Wu, C.; Matz, L. M.; Clowers, B. H.; Seims, W. F.; Hill, H. H. *Anal. Chem.* **2006**, *78*, 8200–8206.
(6) Eckers, C.; Laures, A. M.-F.; Giles, K.; Major, H.; Pringle, S. *Rapid Commun. Mass Spectrom.* **2007**, *21*, 1255–1263.
(7) Kanu, A. B.; Hill, H. H. *J. Chromatogr., A* **2008**, *1177*, 12–27.
(8) McMinn, D. G.; Kinzer, J.; Shumate, C. B.; Siems, W. F.; Hill, H. H. *J. Microcolumn Sep.* **1990**, *2*, 188–192.
(9) Tang, X.; Bruce, J. E.; Hill, H. H. *Anal. Chem.* **2006**, *78*, 7751–7760.
(10) Khayamian, T.; Jafari, M. T. *Anal. Chem.* **2007**, *79*, 3199–3205.
(11) Chen, Y. H.; Hill, H. H. *J. Microcolumn Sep.* **1994**, *6*, 515–524.
(12) Tam, M.; Hill, H. H. *Anal. Chem.* **2004**, *76*, 2741–2747.
(13) Lubinan, D. M.; Kronlck, M. N. *Anal. Chem.* **1983**, *55*, 867–873.
(14) Sielemann, S.; Baumbach, J. I.; Schmidt, H. *Int. J. Ion Mobility Spectrom.* **2002**, *5*, 143–148.
(15) Tabrizchi, M.; Khayamian, T.; Taj, N. *Rev. Sci. Instrum.* **2000**, *71*, 2321–2328.
(16) Xu, J.; Whitten, W. B.; Ramsey, J. M. *Anal. Chem.* **2003**, *75*, 4206–4210.
(17) Ross, S. K.; Bell, A. J. *Int. J. Mass Spectrom.* **2002**, *218*, L1−L6.
(18) Hill, C. A.; Thomas, C. L. P. *Analyst* **2003**, *128*, 55–60.
(19) Andrade, F. J.; Shelley, J. T.; Wetzel, W. C.; Webb, M. R.; Gamez, G.; Ray, S. J.; Hieftje, G. M. *Anal. Chem.* **2008**, *80*, 2654–2663.
(20) Dong, C.; Wang, W.; Li, H. *Anal. Chem.* **2008**, *80*, 3925–3930.
(21) Baim, M. A.; Eatherton, R. L.; Hill, H. H. *Anal. Chem.* **1983**, *55*, 1761–1766.

10.1021/ac100342y
Published on Web 04/16/2010

energy (in most cases, less than 11.7 eV), which indicates the possibility of improving the selectivity of IMS by selecting an ultraviolet radiation wavelength. It cannot ionize common molecules in ambient air (e.g., N_2 (IP, 15.58 eV), O_2 (IP, 12.07 eV), etc.[23]) and thereby reduces possible interferences caused by the reactant ions compared with the ^{63}Ni source. Moreover, ultraviolet radiation is known as a soft ionization method to produce positive molecular ions.[24] It is widely employed as a positive ionization source in IMS for the detection of volatile organic compounds.[25−27] To our knowledge, however, rare work has been performed to develop a negative ionization source by using ultraviolet radiation. In this paper, we introduce a novel ultraviolet radiation ionization (UVRI) source which works as an efficient negative ionization source and meanwhile maintains the capability to work as an positive ionization source.

The core concept of the new UVRI source for negative ion mode is the photoelectric effect whereby electrons eject from a metal surface by ultraviolet radiation with photons of energy exceeding the work function of the metal (in most cases, no bigger than 5.65 eV).[28] The low-energy photoelectrons generated will be captured by electronegative compounds to form negative ions, and thereby no positive ions are produced. In addition, the number of photoelectrons depends on the photon flux of the incident light, permitting the electrons number to be tailored for a particular analysis. Thus, this approach has been used widely in experiments requiring low-energy electrons, such as the development of a nonradioactive electron source with a 4.9 eV UV lamp and a metal foil for an electron capture detector in gas chromatography by Simmonds.[29] A commercial vacuum-UV Kr lamp as an ultraviolet source is extensively used as a direct photoionization source.[21,25] It is characterized as being easy to operate, relatively stable, and a tunable radiation intensity and having low cost. In this UVRI source, a 10.0 eV vacuum-UV Kr lamp with ultraviolet radiation wavelength of 123.6 nm is set to emit low-energy photoelectrons from the surface of a gold mesh for the negative ion mode, and it can also be used under positive ion mode. In addition, early studies of the stratospheric O_3 showed that short-wavelength ultraviolet radiation (103 nm < λ < 190 nm) can photosplit O_2 and initiate O_3 formation,[30,31] and this approach had already been used for ozone production.[32,33] In the UVRI source, since the ultraviolet radiation comes from electric discharge inside the vacuum-UV lamp and N_2 gas is almost transparent to this ultraviolet radiation,[34,35] clean O_3 molecules without NO_x contamination are produced by the vacuum-UV lamp in purified air, which is different from a corona discharge ionization source.[17] Considering the greater electron affinity (EA) of O_3 compared to that of O_2 (O_3 (EA, 2.10 eV), O_2 (EA, 0.45 eV)[23]), the simultaneous production of O_3 molecules and photoelectrons in the new source may form new reactant ions, $O_3^-(H_2O)_n$, for its negative ion mode. On the other hand, the reactant ions for the negative ion mode of the ^{63}Ni source in purified air are dominated by $O_2^-(H_2O)_n$.[1,36,37]

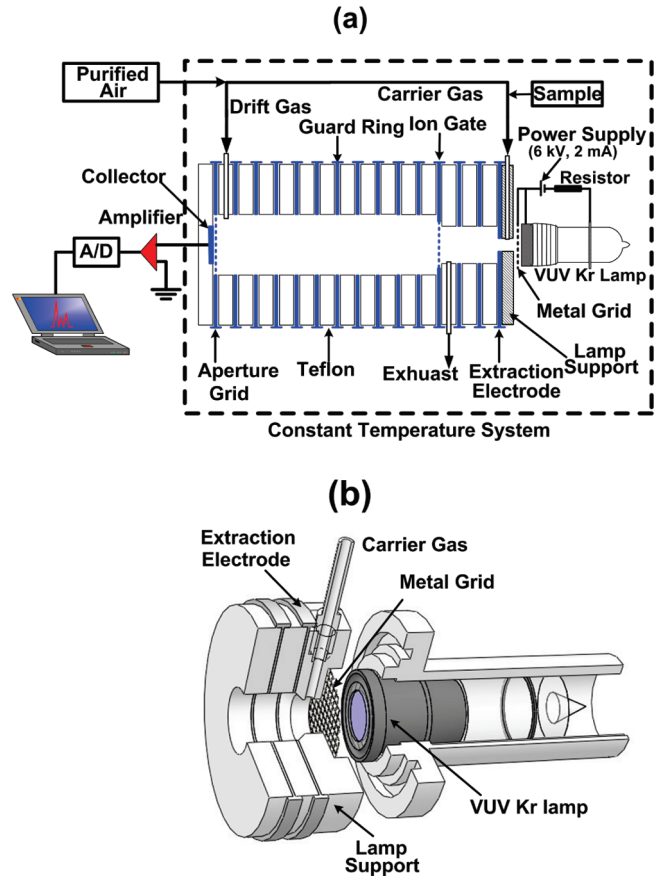

Figure 1. (a) Schematic diagram of the UVRI-IMS apparatus. (b) Design of the UVRI source.

This paper is organized as follows: First, a description of this new UVRI source is given in detail. Second, experimental verification of the reactant ions in negative ion mode is implemented. Third, sensitive measurements of some inorganic molecules using the new reactant ions under negative mode are demonstrated. Finally, the performances of the UVRI source as an efficient negative ionization source and as an ordinary photoionization positive ion source are presented.

EXPERIMENTAL SECTION

Apparatus. A schematic diagram of the ion mobility spectrometer is shown in Figure 1a, and its main features are outlined

(22) Leasure, C. S.; Fleischer, M. E.; Anderson, G. K.; Eiceman, G. A. *Anal. Chem.* **1986**, *58*, 2142–2147.
(23) http://webbook.nist.gov/chemistry/.
(24) Nazarov, E. G.; Miller, R. A.; Eiceman, G. A.; Stone, J. A. *Anal. Chem.* **2006**, *78*, 4553–4563.
(25) Sielemann, S.; Baumbach, J. I.; Schmidt, H.; Pilzecker, P. *Field Anal. Chem. Technol.* **2000**, *4*, 157–169.
(26) Baumbach, J. I.; Sielemann, S.; Xie, Z.; Schmidt, H. *Anal. Chem.* **2003**, *75*, 1483–1490.
(27) Sielemann, S.; Baumbach, J. I.; Schmidt, H.; Pilzecker, P. *Anal. Chim. Acta* **2001**, *431*, 293–301.
(28) Sommer, A. H. *Photoemissive Materials*, 1st ed.; Wiley: New York, 1968.
(29) Simmonds, P. G. *J. Chromatogr.* **1987**, *399*, 149–164.
(30) Eliasson, B.; Kogelschatz, U. *Ozone Sci. Eng.* **1991**, *13*, 365–373.
(31) Ivanov, V. V.; Popov, N. A.; Proshina, O. V.; Rakhimova, T. V.; Rulev, G. B.; Saenko, V. B. *Tech. Phys. Lett.* **2001**, *27*, 29–31.
(32) Obenshain, D. N. Vestvaco Corp., New York, NY, U.S. Patent 4329212, 1982.
(33) Salvermoser, M. J.; Kogelschatz, U.; Murnick, D. E. *Eur. Phys. J. Appl. Phys.* **2009**, *47*, 1–6.
(34) Herzberg, G. *Molecular Spectra and Molecular Structure, I. Spectra of Diatomic Molecules*, 3rd ed.; Van Nostrand: New York, 1953.
(35) Meier, R. R. *Space Sci. Rev.* **1991**, *58*, 1–185.
(36) Spangler, G. E.; Collins, C. I *Anal. Chem.* **1975**, *47*, 393–402.
(37) Hayhurst, C. J.; Watts, P.; Wilders, A. *Int. J. Mass Spectrom. Ion Processes* **1992**, *121*, 127–139.

here. The IMS tube was constructed from a series of stacked stainless steel guard rings separated by Teflon insulating rings, with a reaction region of 22 mm long and a drift region of 88 mm long. The inner diameters of the reaction and drift regions were 14 and 30 mm, respectively. A high-voltage direct current (DC) power supply (5000 V, 2 mA) was used to provide a constant high voltage for the extraction electrode of the ion drift tube. This voltage dropped to ground via a series of 1 MΩ resistors (not shown in Figure 1a) which were connected to each of the guard rings. Thus, a homogeneous electrical field of 242.5 V/cm was maintained in the ion drift region. The ion gate was a Bradbury−Nielson type with an injection pulse of 200 μs under current conditions. Ions were separated in the ion mobility drift region according to their reduced mobility values (K_o values1) and received by the collector. The ion current received by the collector was enlarged by an amplifier with a gain of 10^9 V/A and then was fed to a computer via an A/D converter.

The details of the UVRI source are shown in Figure 1b. It was mainly comprised of three parts: a vacuum-UV lamp, a lamp support, and a metal grid. A 10.0 eV vacuum-UV Kr lamp (Cathodeon Ltd., Cambridge, U.K.) was used to provide the ultraviolet photon with wavelength of 123.6 nm. The cylindrical lamp support was made of machinable ceramics with a length of 6 mm and an inner diameter of 10.0 mm. The metal grid (Buckbee-Mears Cortland Co. Inc., Cortland, NY) located between the lamp and the lamp support was made of gold with a diameter of 20 mm and transmissivity of 78%. A second high-voltage DC power supply (6000 V, 2 mA) with a ballast resistor (2−50 MΩ) was set to ignite the lamp and provide a voltage to the gold grid higher than that of the extraction electrode. Positive or negative ions generated in the UVRI source were introduced into the reaction region of the IMS due to the voltage difference U_d between the gold grid and extraction electrode. For comparison, a 10 mm long cylindrical 12 mCi ^{63}Ni source (Beijing Atom High-Tech Co., Ltd.) with an inner diameter of 10 mm was equipped to the IMS tube described above to construct ^{63}Ni IMS with all other parameters remaining the same with UVRI-IMS.

A bidirectional flow scheme was adopted in our IMS instrument, and samples were directly carried into the reaction region by carrier gas. The carrier and drift gases were compressed air purified by activated carbon, silica gel, and freshly baked 13X molecular sieves trap with a total length of 3 m to efficiently remove the impurities, CO_2, and water vapors, etc. The flow rates for carrier and drift gases were 400 and 600 mL/min, respectively. The moisture of the purified air was monitored by a dew point instrument (DP300, CS Instrument GMH) and fixed below 1 ppmv. Except noted, all the joints and connections of our IMS instrument were carefully sealed, and the temperature of the whole system (encompassed by dotted line, Figure 1a) was always fixed at 30.5 °C except for the case of detecting explosives, which was fixed at 150 °C.

The reduced mobility values (K_o values) in the text were calculated via the following equation:[1]

$$K_o = \frac{d}{Et_d}\frac{273.5}{T}\frac{P}{760} \quad (1)$$

where d is the length of the ion mobility drift region (8.8 cm), E is the electric field strength of the ion mobility drift region (242.5 E/cm), t_d is the drift time of the species (ms), T is the temperature of the ion mobility tube (304 or 423.5 K), and P is the gas pressure (760 Torr).

Sample Preparation and Methods. Standard gases of 500 ppmv CO_2 in the mixture of 78% N_2 (99.9995% purity) and 22% O_2 (99.9996% purity), 500 ppmv H_2S in N_2 (99.9995% purity), and 500 ppmv SO_2 in N_2 (99.9995% purity) were all purchased from Dalian Special Gas Co., Ltd. (Dalian, China). All the samples with different concentrations of SO_2, H_2S, or CO_2 were obtained by diluting their standard gases with the purified air in a mixing chamber. The flow rates of standard gas and the purified air were controlled by mass flow controllers (Seven Star Electronics Co., Ltd., Beijing, China) at calculated flux proportion, respectively. Benzene, toluene, *m*-xylene, and acetone were all analytical grade and purchased from Kermel Chemicals Co., Ltd. (Tianjin, China). Benzene, toluene, and *m*-xylene with different concentrations were obtained by diluting the headspace vapor of an 80 mL flask with purified air, inside of which there is a 2 mL vessel loaded with 1 mL of pure sample. The vessel was sealed by capsule, and the concentration of the sample in the headspace of the flask was controlled by regulating the capsule and could be calculated by a weighting method.

Cyclo-1,3,5-trimethylene-2,4,6-trinitramine (RDX), pentaerythritol tetranitrate (PETN), *N*-nitrobis(2-hydroxyethyl)amine dinitrate (DINA), and ammonium nitrate fuel oil explosive (ANFO) were all commercial grade. Explosives with different concentrations in acetone were prepared by successive dilution of their stock solutions with concentration of 1 ng/μL in acetone.

Safety Considerations. Extreme cares should be taken to avoid electrical shock in operation with a high-voltage power supply. Sulfide compounds, benzene series compounds, and nitroexplosives are known toxins or carcinogens and should be handled with gloves in a fume hood. Skin and eye contact and accidental inhalation and ingestion should be avoided.

RESULTS AND DISCUSSION

Ion Intensity. The voltage difference U_d between the gold grid and the extraction electrode can affect the transmission efficiency of the ions from the UVRI source to the reaction region of the IMS tube by adjusting the voltage on the gold grid. Figure 2a shows the evolution of the integrated intensity of the reactant ion peak (RIP) in negative ion mode is a function of U_d. The integrated intensity of the RIP grows with the increase of U_d in the beginning and approaches a plateau after U_d reaches 1000 V. It seems that the U_d dramatically affects the ion transmission efficiency when U_d is lower than 1000 V. When $U_d = 0$ V, the integrated intensity of RIP is still about 600 au, which indicates some ions may enter into the reaction region by coulomb repulsion. From Figure 2a, the effect of the vacuum-UV Kr lamp operating current on the integrated intensity RIP is also extracted. With U_d fixed, the integrated intensity of the RIP rises with the increase of the lamp operating current. For instance, when U_d is fixed at 1000 V, the integrated intensity of the RIP rises from 1150 to 3600 au as the lamp operating current rises from 0.1 to 0.6 mA. This may be due to the increase of the photon flux of ultraviolet radiation as the lamp operating current increases, which leads to more electrons being released from the gold mesh. This phenomenon indicates

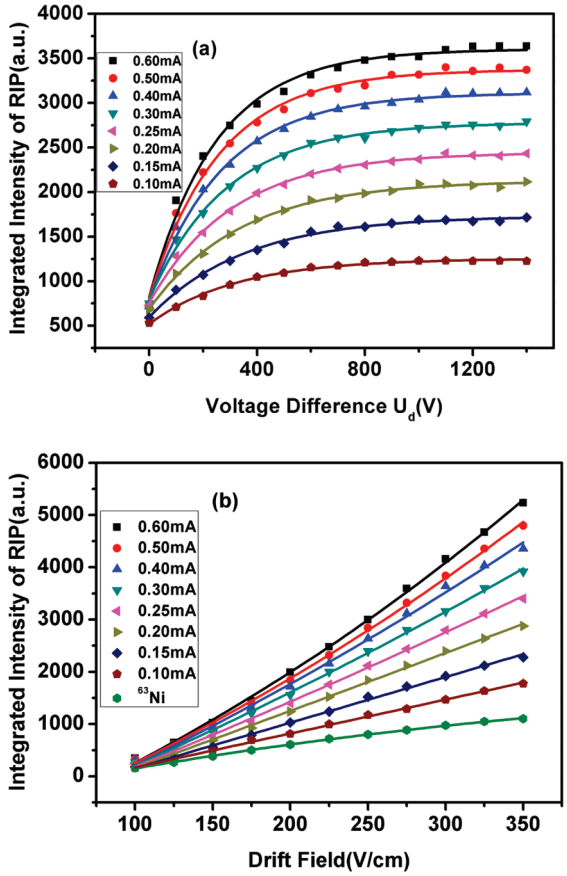

Figure 2. (a) Plots of the integrated intensity of reactant ion peak (RIP) versus the voltage difference U_d for the UVRI source in negative ion mode. (b) Plots of the integrated intensity of RIP versus the drift field for the UVRI and the ^{63}Ni sources in negative ion mode with U_d at 1000 V.

the possibility in flexibly tuning the reactant ion intensity by adjusting the working current of the vacuum-UV lamp.

When U_d is fixed at 1000 V, the evolutions of the RIP integrated intensity versus the drift field with the UVRI and ^{63}Ni sources under negative ion mode are shown in Figure 2b. The increased amplitude is more remarkable for the UVRI source, especially from 200 to 5500 au at lamp operating current of 0.6 mA, while, for the ^{63}Ni source, just from 120 to 1000 au. It is noted that the integrated intensities of the RIP for the UVRI source are higher than that of the ^{63}Ni source within the lamp operating current range from 0.1 to 0.6 mA under the same drift field, normally by a factor of 1.5−5. The stability of this new UVRI source was also studied by monitoring the evolution of the integrated intensity of the RIP; the results showed that the relative standard deviation is lower than 0.66% in a range of 180 min.

Negative Reactant Ions. Ion mobility spectra for purified air with the UVRI and ^{63}Ni sources under negative ion mode are shown in Figure 3. Parts a and b of Figure 3 show distinctive reactant ion peaks with corresponding K_o values of 2.55 and 2.38 cm^2 V^{-1} s^{-1}, which indicate the different reactant ions in the UVRI and ^{63}Ni sources. The negative reactant ions in the ^{63}Ni source are commonly recognized as hydrated O_2^- anions. In the UVRI source, when the vacuum-UV lamp was illumined, low-energy photoelectrons were released from the surface of the gold grid and O_3 molecules were generated. The O_3

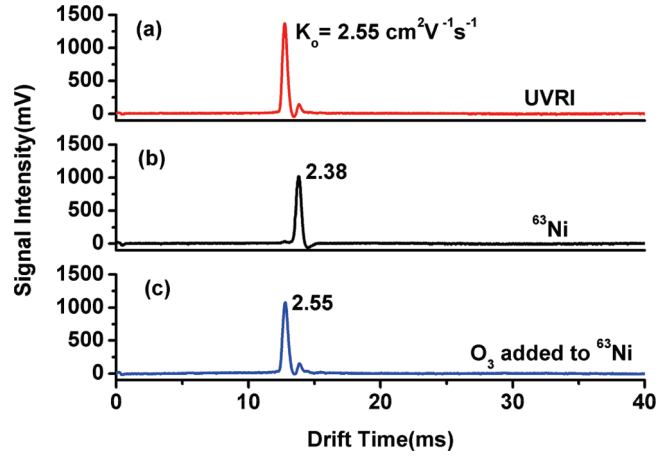

Figure 3. Negative ion mobility spectra of purified air with (a) the UVRI source, (b) the ^{63}Ni source, and (c) the ^{63}Ni source when purified air with 1700 ppmv O_3 was used as the carrier gas.

concentration was measured to be about 1700 ppmv using the iodometric titration method. The low-energy photoelectrons could be quickly captured by O_2 and O_3 molecules to form O_2^- and O_3^- anions (eq 3 and eq 4)[38] which would further cluster water molecules to form their hydrated anions (eq 5 and eq 6).

$$\text{metal} + h\nu \rightarrow e^- \quad (2)$$

$$e^- + O_2 + M \rightarrow O_2^- + M \quad (M = N_2, O_2, H_2O, \text{etc.}) \quad (3)$$

$$e^- + O_3 + M \rightarrow O_3^- + M \quad (4)$$

$$O_2^- + nH_2O + M \rightarrow O_2^-(H_2O)_n + M \quad (5)$$

$$O_3^- + nH_2O + M \rightarrow O_3^-(H_2O)_n + M \quad (6)$$

The initially formed $O_2^-(H_2O)_n$ could ultimately convert to $O_3^-(H_2O)_n$ through charge-transfer reaction (eq 7),[39] and consequently distinctive anions, hydrated O_3^-, were formed in this source.

$$O_2^-(H_2O)_n + O_3 \rightarrow O_3^-(H_2O)_{n-1} + O_2 + H_2O \quad (7)$$

In addition, the calculated K_o values for the reactant ion peaks from the UVRI and ^{63}Ni sources are 2.55 and 2.38 cm^2 V^{-1} s^{-1} consistent with the previously reported K_o values of 2.56 and 2.31 cm^2 V^{-1} s^{-1} for $O_3^-(H_2O)_n$ and $O_2^-(H_2O)_n$ by McKnight[40] and Kimura et al.[41] Thus, it is reasonable to assign the negative reactant ions in the UVRI source to be $O_3^-(H_2O)_n$.

To verify the above assumption, purified air with O_3 concentration of 1700 ppmv was used as the carrier gas of IMS with ^{63}Ni source, and the result is shown in Figure 3c. As can be

(38) Begley, P.; Corbin, R.; Foulger, B. E.; Simmonds, P. G. *J. Chromatogr.* **1991**, *588*, 239–249.
(39) Fahey, D. W.; BoHringer, H.; Fehsenfeld, F. C.; Ferguson, E. E. *J. Chem. Phys.* **1982**, *76*, 1799–1805.
(40) McKnight, L. G. *Phys. Rev. A* **1970**, *2*, 762–770.
(41) Kimura, T.; Hayashi, T.; Suzuki, S.; Itoh, H. *XXVIIth ICPIG*; Eindhoven, The Netherlands, 2005.

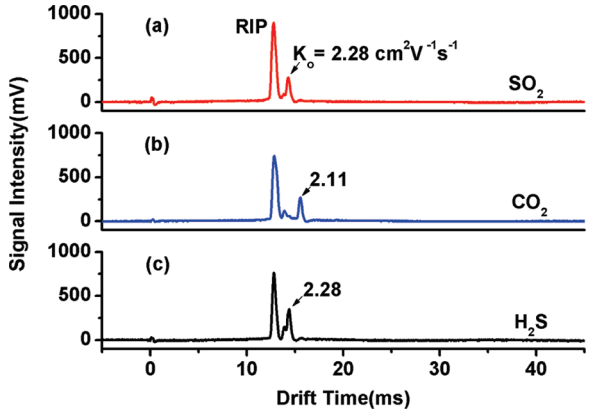

Figure 4. Negative ion mobility spectra for (a) 100 ppbv SO_2, (b) 150 ppmv CO_2, and (c) 200 ppbv H_2S with the UVRI source (RIP, reactant ion peak).

seen from Figure 3c, a new peak appears with K_o value of 2.55 $cm^2\ V^{-1}\ s^{-1}$, which is the same as that of the reactant ion peak in Figure 3a. In comparison with the spectrum shown in Figure 3b, this result indicates that when O_3 was introduced into the ^{63}Ni source, the charge-transfer reaction between O_3 and $O_2^-(H_2O)_n$ certainly occurred, and the $O_2^-(H_2O)_n$ was converted to $O_3^-(H_2O)_n$ completely. So, we are convinced that the reactant ions for the UVRI source is predominantly ascribed to be $O_3^-(H_2O)_n$.

Detection of Inorganic Molecules. Inorganic molecules such as SO_2, CO_2, and H_2S play an important role in the atmospheric environment. Figure 4 shows the ion mobility spectra for 100 ppbv SO_2, 150 ppmv CO_2, and 200 ppbv H_2S obtained by using the UVRI source under negative ion mode. The ion mobility spectrum for SO_2 (Figure 4a) shows only one product ion peak with a calculated K_o value of 2.28 $cm^2\ V^{-1}\ s^{-1}$. For SO_2, its lower EA compared with O_3 as well as the high IP indicates that it could not undergo charge-transfer reaction or photoionization in this ionization source (SO_2 (IP, 12.35 eV; EA, 1.107 eV)[23]). The product ion peak for SO_2 may be produced through exothermic O^--transfer reaction between $O_3^-(H_2O)_n$ and SO_2 (eq 8).[42,43] This is a well-known reaction with a fast reaction rate ($k = 1.9 \times 10^{-9}$ $cm^3\ s^{-1}$), which led to the production of $SO_3^-(H_2O)_n$ anions and was followed by a rapid conversion of $SO_3^-(H_2O)_n$ to $SO_5^-(H_2O)_n$ in the presence of O_2 (eq 9).[44]

$$O_3^-(H_2O)_n + SO_2 \rightarrow SO_3^-(H_2O)_m + O_2 + (n - m)H_2O \quad (8)$$

$$SO_3^-(H_2O)_n + O_2 \rightarrow SO_5^-(H_2O)_n \quad (9)$$

Thus the product ion peak for SO_2 could be tentatively ascribed to $SO_5^-(H_2O)_n$ anions. In Figure 4, the ion mobility spectrum of CO_2 (Figure 4b) also shows one product ion peak with a calculated K_o value of 2.11 $cm^2\ V^{-1}\ s^{-1}$. In view of its high IP and negative EA, the product ion peak of CO_2 here may also be produced via the exothermic O^--transfer reaction between CO_2 and $O_3^-(H_2O)_n$ (eq 10),[42] thereby being tentatively ascribed to $CO_3^-(H_2O)_n$ (CO_2 (IP, 13.78 eV; EA, −0.45 eV)[23]).

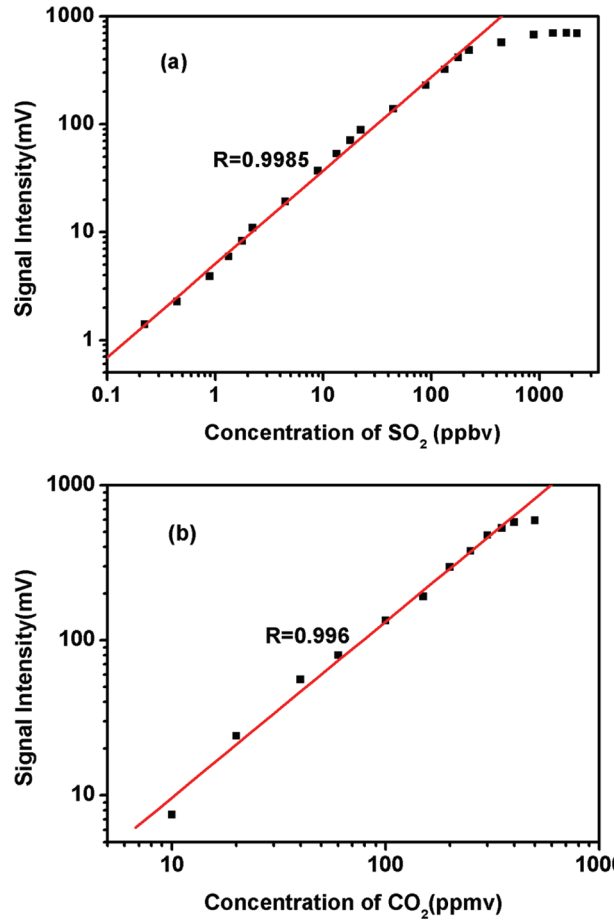

Figure 5. Plots of product ion signal intensity versus concentration for (a) SO_2 and (b) CO_2.

$$O_3^-(H_2O)_n + CO_2 \rightarrow CO_3^-(H_2O)_n + O_2 \quad (10)$$

For H_2S, also only one product ion peak was observed (Figure 4c) with a calculated K_o of the same value as that for SO_2. This is probably ascribed to the oxidation−reduction reaction between H_2S and O_3 (eq 11),[23] whereby SO_2 was produced when H_2S was introduced into this ionization source.

$$H_2S + O_3 \rightarrow SO_2 + H_2O \quad (11)$$

So, here the product ion peak for H_2S is also ascribed to $SO_5^-(H_2O)_n$ anions.

Plots of product ion peak intensity detected versus the concentration for SO_2 and CO_2 are shown in Figure 5. Due to the lack of standard H_2S sample, its response curve was not collected. In Figure 5a, the response curve for SO_2 shows a linear increase range from 220 pptv to 220 ppbv, about 3 orders of magnitude. The calculated limit of detection (LOD) (S/N = 3) for SO_2 was about 150 pptv. In other work, the LOD of 2 ppb for SO_2 was previously reported using ^{63}Ni IMS in air by

(42) Albriton, D. L.; Dotan, I.; Streit, G. E.; Fahey, D. W.; Fehsenfeld, F. C.; Ferguson, E. E. *J. Chem. Phys.* **1983**, *78*, 6614–6619.
(43) Mohler, O.; Reiner, T.; Arnold, F. *J. Chem. Phys.* **1992**, *97*, 8233–8239.
(44) Salcedo, D.; Villalta, P. W.; Varutbangkul, V.; Wormhoudt, J. C.; Miake-Lye, R. C.; Worsnop, D. R.; Ballenthin, J. O.; Thorn, W. F.; Viggiano, A. A.; Miller, T. M.; Flagan, R. C.; Seinfeld, J. H. *Int. J. Mass Spectrom.* **2004**, *231*, 17–30.

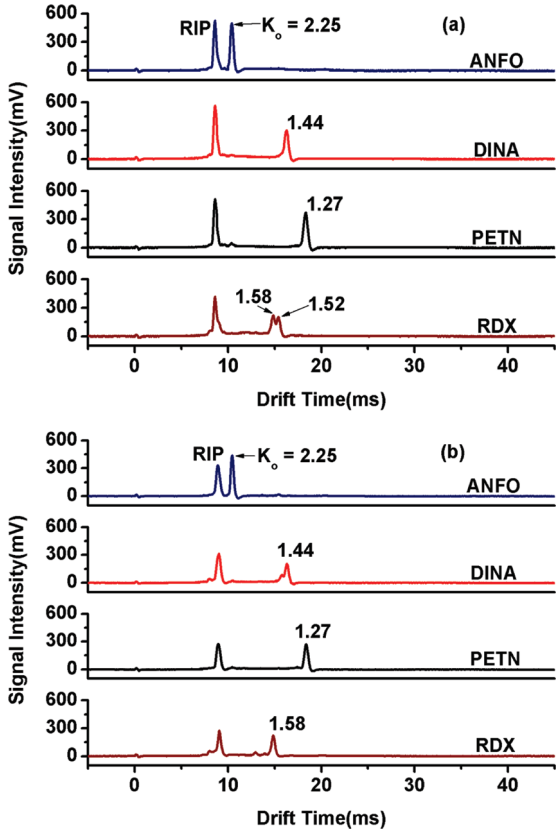

Figure 6. Ion mobility spectra of 10 ng of ANFO, 10 ng of DINA, 10 ng of PETN, and 10 ng of RDX acquired by employing (a) the UVRI-IMS and (b) the ^{63}Ni IMS under negative ion mode at 150 °C.

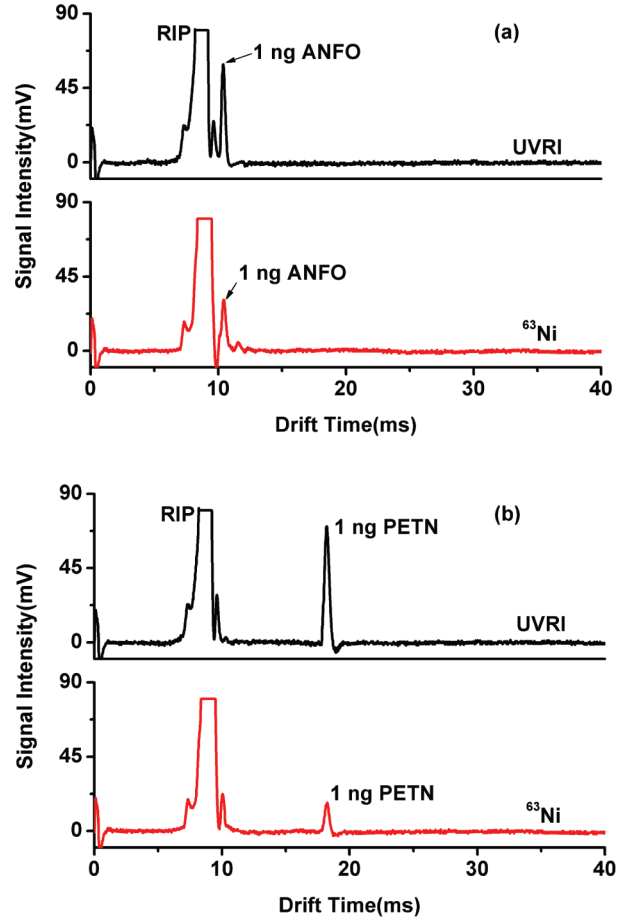

Figure 7. Comparison of the signal intensities of (a) 1 ng of ANFO and (b) 1 ng of PETN acquired by using the UVRI-IMS and the ^{63}Ni IMS under negative ion mode at 150 °C.

Eiceman et al.[45] For CO_2, its response curve shows a linear increase range of about one and a half orders of magnitude from 10 to 450 ppmv, and the calculated LOD for CO_2 was about 1 ppmv. In the early work performed by Spangler and Collins,[36] the response characteristics of CO_2 with different concentration in ^{63}Ni IMS had been investigated, but no obvious product ion peak for CO_2 was observed.

Applications of UVRI-IMS. One of the important applications of IMS is the detection of explosives. Here, the performance of the UVRI-IMS in detecting explosives under negative ion mode was investigated. The ion mobility spectra for 10 ng of ANFO, 10 ng of DINA, 10 ng of PETN, and 10 ng of RDX acquired by employing the UVRI source at 150 °C are shown in Figure 6a. For comparison, their ion mobility spectra acquired with ^{63}Ni source at the same conditions are shown in Figure 6b. In Figure 6a, the ion mobility spectra of ANFO, DINA, and PETN all show only one sharp product ion peak with calculated K_o values of 2.25, 1.44, and 1.27 cm^2 V^{-1} s^{-1}, respectively, which are the same as those in Figure 6b. These product ion peaks should be produced via decomposition of ANFO, DINA, and PETN at high temperature,as described by Ewing et al.,[46] and correspond to NO_3^-, PETN·NO_3^-, and DINA·NO_3^- anions, respectively. In Figure 6a, two product ion peaks are observed in the spectrum for RDX with calculated K_o values of 1.58 and 1.52 cm^2 V^{-1} s^{-1}. However, in Figure 6b, there is only one product ion peak for RDX with a calculated K_o value of 1.58 cm^2 V^{-1} s^{-1}, and this product ion peak should correspond to RDX·NO_2^- anions according to the description of Ewing et al.[46] The difference between the spectra for RDX acquired with the UVRI source and the ^{63}Ni source should be ascribed to the existence of a high concentration O_3 molecules in the UVRI source. Some of the NO_2^- ions fragmented by RDX were converted to NO_3^- ions in the UVRI source, and then these anions associated with RDX molecules to produce RDX·NO_2^- and RDX·NO_3^- ions. When NH_4NO_3 was added to RDX, a sharp increase emerged for the product ion peak with a K_o value of 1.52 cm^2 V^{-1} s^{-1}. Thus, the product ion peaks of RDX with K_o values of 1.58 and 1.52 cm^2 V^{-1} s^{-1} are tentatively ascribed to RDX·NO_2^- and RDX·NO_3^-, respectively.

For explosives, the product ion peak heights for ANFO, DINA, RDX, and PETN with the UVRI source were greater than that with the ^{63}Ni source. As demonstrated by Figure 7a, for 1 ng of ANFO the peak height with the UVRI source is about 59 mV, almost 2 times that of 29 mV with the ^{63}Ni source. And for 1 ng of DINA and RDX the peak heights with the UVRI source were about 2 times and 1.5 times those with the ^{63}Ni source. While for PETN, a better enhanced sensitivity was observed. In Figure 7b, the peak height for 1 ng of PETN with the UVRI source is about 70 mV, while the peak height with the ^{63}Ni source is only about 15 mV, more than 4 times enhanced. Using exponential

(45) Eiceman, G. A.; Leasure, C. S.; Vandiver, V. J. *Anal. Chem.* **1986**, *58*, 76–80.
(46) Ewing, R. G.; Atkinson, D. A.; Eiceman, G. A.; Ewing, G. J. *Talanta* **2001**, *54*, 515–529.

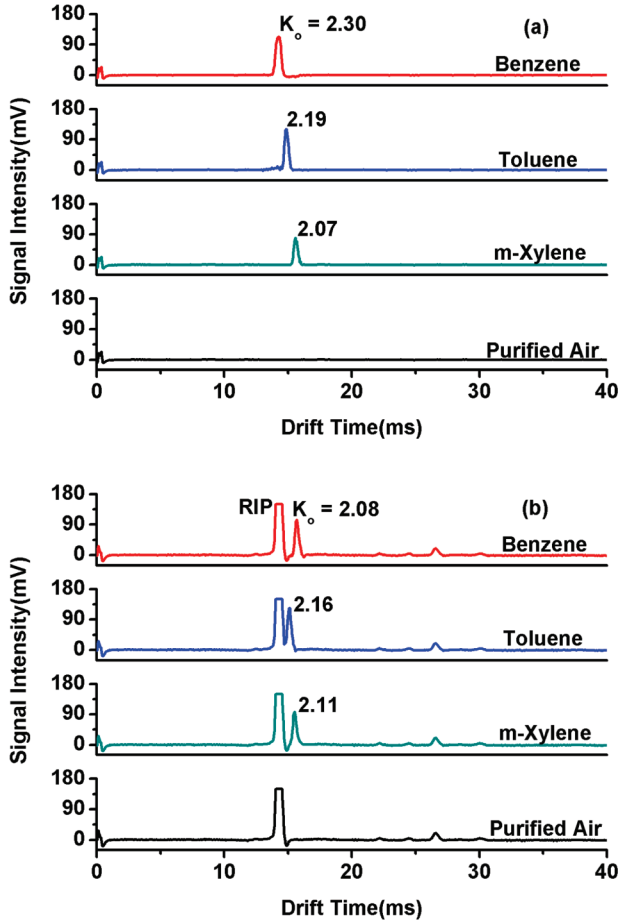

Figure 8. Ion mobility spectra of 450 ppbv benzene, 400 ppbv toluene, 300 ppbv *m*-xylene, and purified air acquired by (a) the UVRI-IMS and (b) the ^{63}Ni IMS under positive ion mode.

dilution method,[47] the LOD obtained for PETN with the UVRI source was about 45 pg. However, with the ^{63}Ni source under the same experimental condition the LOD was about 190 pg.

Under positive ion mode, the performance of the UVRI-IMS in detecting aromatic compounds, such as benzene, toluene, and *m*-xylene, was investigated. Figure 8a shows the ion mobility spectra for 450 ppbv benzene, 400 ppbv toluene, and 300 ppbv *m*-xylene acquired by UVRI-IMS, and a sharp product ion peak can be clearly seen in each spectrum. The calculated K_o values are 2.30 cm^2 V^{-1} s^{-1} for benzene, 2.19 cm^2 V^{-1} s^{-1} for toluene, and 2.07 cm^2 V^{-1} s^{-1} for *m*-xylene, which are consistent with the literature values of 2.27, 2.13, and 2.05 cm^{2}V^{-1}s^{-1} by using the photoionization source.[25] Thus, these product ion peaks are tentatively ascribed to $C_6H_6^+(H_2O)_n$, $C_7H_8^+(H_2O)_n$, and $C_8H_{10}^+(H_2O)_n$, respectively. For comparison, the ion mobility spectra for 450 ppbv benzene, 400 ppbv toluene, and 300 ppbv *m*-xylene acquired by employing ^{63}Ni IMS are shown in Figure 8b, where also only one product ion peak is observed for each compound with calculated K_o values of 2.08, 2.16, and 2.11 cm^2 V^{-1} s^{-1}, respectively. These product ion peaks correspond to $C_6H_7^+(H_2O)_n$, $C_7H_9^+(H_2O)_n$, and $C_8H_{11}^+(H_2O)_n$ ions according to the assignment of Eiceman and Karpas.[1]

(47) Spangler, G. E.; Lawless, P. A. *Anal. Chem.* **1978**, *50*, 884–892.

As shown in Figure 8a, the product ion peak heights for benzene, toluene, and *m*-xylene with the UVRI source are about 105, 110, and 70 mV, comparable to that shown in Figure 8b which are 100, 120, and 92 mV with the ^{63}Ni source. Using exponential dilution method,[47] the LODs for benzene, toluene, and *m*-xylene obtained with the UVRI source were about 63, 55, and 50 ppbv, and that with the ^{63}Ni source were about 65, 60, and 40 ppbv. This result may indicate a comparable performance of the UVRI-IMS and the ^{63}Ni IMS in detecting benzene series compounds under positive ion mode. In addition, the ion mobility spectrum for purified air employing the UVRI-IMS is also shown in Figure 8a, where only a smooth straight baseline without any ion peak is observed. This demonstrates that the UVRI source holds the advantage of reducing possible interferences caused by the reactant ions compared with the ^{63}Ni source. In light of these results, we may conclude that the UVRI source can also work as a normal photoionization source very well.

CONCLUSIONS

In this work, a novel bipolar ionization source for ion mobility spectrometry has been introduced. It can work under negative ion mode and positive ion mode. Comparing to the traditional ^{63}Ni ionization source, an additional power supply and periodically replacing the lamp due to its finite lifetime are required. Nevertheless, this new source exhibits excellent performance. In this new source, distinctive reactant ions under negative ion mode were detected and predominantly assigned to $O_3^-(H_2O)_n$. Proof-in-principle applications of the new ionization possibility of $O_3^-(H_2O)_n$ were implemented by sensitive detection of inorganic molecules SO_2, CO_2, and H_2S, and a linear dynamic range of 3 orders of magnitude and a limit of detection ($S/N = 3$) of 150 pptv were obtained for SO_2. Preliminary application in the detection of common explosives at 150 °C showed good sensitivity, and the LOD was reached for 45 pg of PENT. Its performance as an ordinary photoionization source was also shown in the detection of benzene series compounds. However, much more needs to be investigated in the future, for example, verification of the reactant ions by combining the ion mobility spectrometer with a time-of-flight mass spectrometer and its applications in the detection of other important volatile organic compounds.

ACKNOWLEDGMENT

Financial support from National Natural Science Foundation of China (Grant Nos. 20877074, B070102, 40639036), National High-Tech Research and Development Plan (Grant No. 2007AA-061503), and Instrument Developing Project of the Chinese Academy of Sciences (Grant No. YZ200907) is gratefully acknowledged. The authors acknowledge the People's Public Security University of China for providing the explosive material.

Received for review February 7, 2010. Accepted April 1, 2010.

AC100342Y